Dynamic similarity and scale effects affecting air bubble entrainment in hydraulic jumps

Hubert Chanson

The University of Queensland, Div. of Civil Engineering
Brisbane Qld 4072, Australia
E-mail: h.chanson@uq.edu.au

Keywords: hydraulic jumps, air bubble entrainment, dynamic similarity, scale effects, physical modelling

Abstract

In an open channel, the transition from super- to sub-critical flow is a flow singularity (the hydraulic jump) characterised by a sharp rise in free-surface elevation, strong turbulence and air entrainment in the roller. A key feature of the hydraulic jump flow is the strong free-surface aeration and air-water flow turbulence. In the present study, similar experiments were conducted with identical inflow Froude numbers Fr_1 using a geometric scaling ratio of 2:1. The results of the Froude-similar experiments showed some drastic scale effects in the smaller hydraulic jumps in terms of void fraction, bubble count rate and bubble chord time distributions. Void fraction distributions implied comparatively greater detrainment at low Reynolds numbers yielding some lesser aeration of the jump roller. The dimensionless bubble count rates were significantly lower in the smaller channel, especially in the mixing layer. The bubble chord time distributions were quantitatively close in both channels, and they were not scaled according to a Froude similitude. Simply the hydraulic jump remains a fascinating two-phase flow motion that is still poorly understood.

Introduction

In an open channel, the transition from super- to sub-critical flow is a flow singularity, called hydraulic jump, that is characterised by a sharp rise in free-surface elevation, strong turbulence and air entrainment in the roller (Fig. 1). Although the hydraulic jump equations were solved during the early 19th century (Bélanger 1829), the air bubble entrainment processes were not investigated until the mid-20th century. The first reports into air bubble entrainment in hydraulic jumps investigated the air demand in closed-conduits: i.e., the total quantity of entrained air (e.g. Kalinske and Robertson 1943, Wisner 1965). Basic studies of bubble entrainment in hydraulic jumps started with Rajaratnam (1962) and Thandaveswara (1974) in India. A 'milestone' contribution was the work of Resch and Leutheusser (1972) who showed first that the bubble entrainment process, momentum transfer and energy dissipation are strongly affected by the inflow conditions. Chanson (1995) studied particularly the air-water properties in partially-developed hydraulic jumps, showing some similarity with air entrainment in plunging jets. Mossa and Tolve (1998) recorded instantaneous properties of bubbly flow structures using an imaging technique. Chanson and Brattberg (2000) documented the vertical distributions of void fractions, bubble count rates and air-water velocities in the shear layer and roller region of hydraulic jumps with relatively large inflow Froude numbers. Murzyn et al. (2005) measured detailed air-water flow properties in hydraulic jumps with low inflow Froude numbers.

Although the hydraulic jump has been investigated experimentally for nearly two centuries, little information is available on the air-water flow properties in the jump flow and on the scale effects affecting the air entrapment and advection processes. It is the purpose of this work to present new experiments repeated in two flumes with identical inflow Froude numbers and relative channel widths. The results provide new detailed information on scale effects affecting void fraction, bubble count rate and chord time distributions.

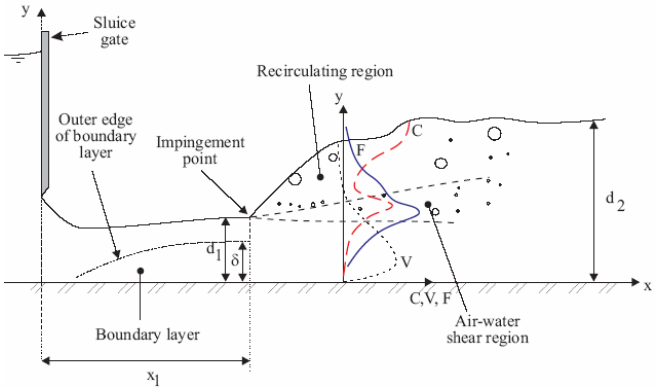

Figure 1: Sketch of air bubble entrainment at a hydraulic jump with partially-developed inflow.

Nomenclature

C	void fraction
C_{max}	maximum void fraction in the air bubble diffusion layer
ch	bubble/droplet chord size (m)
D_t	air bubble diffusivity (m^2/s)

D_t'	air bubble diffusivity (m^2/s) in the upper free-surface region
$D^{\#}$	dimensionless air bubble diffusivity $D^{\#} = D_t/(V_1 \times d_1)$
d_1	inflow depth (m)
d_2	downstream conjugate depth (m)
d_{ab}	bubble size (m)
F	bubble count rate (Hz)
Fr_1	inflow Froude number $Fr_1 = V_1 / \sqrt{g \times d_1}$
F_{max}	maximum bubble count rate (Hz) in the advective diffusion layer
F_{scan}	sampling rate (Hz)
F_{toe}	jump toe fluctuation frequency (Hz)
g	gravitational constant (m/s^2)
L_r	geometric scaling ratio defined as the ratio of prototype to model dimensions
Mo	Morton number $Mo = g \times \mu_w^4/(\rho_w \times \sigma^3)$
N_{ab}	total number of detected bubbles
Q_{air}	volume flow rate of entrained air (m^3/s)
Q_w	water discharge (m^3/s)
Re_1	inflow Froude number $Re_1 = \rho_w \times V_1 \times d_1 / \mu_w$
T_{scan}	sampling duration (s)
u'	characteristic turbulent velocity
V	velocity (m/s)
V_1	inflow velocity (m/s)
W	channel width (m)
x	longitudinal distance from the channel intake (m)
x_1	distance between channel intake and jump toe (m)
Y_{Cmax}	location (m) where $C = C_{max}$
Y_{Fmax}	location (m) where $F = F_{max}$
Y_{50}	characteristic depth where C = 0.50 (m)
y	vertical elevation above the bed (m)
z	transverse distance from the centreline (m)

Greek letters

δ	developing boundary layer thickness (m)
μ	dynamic viscosity (Pa s)
ρ	density (kg/m^3)
σ	surface tension between air and water (N/m)

Subscripts

air	air property
w	water property
1	inflow conditions

Dimensional Analysis and Dynamic Similarity

Theoretical and numerical studies of air bubble entrainment in hydraulic jumps are difficult because of the large number of relevant equations. Experimental investigations of air-water flows are performed with geometrically similar models, based upon a dimensional analysis and dynamic similitude. For a hydraulic jump in a horizontal, rectangular channel, a simplified dimensional analysis shows that the parameters affecting the air-water flow properties at a position (x, y, z) are : (a) the fluid properties including the air and water densities ρ_{air} and ρ_w, the air and water dynamic viscosities μ_{air} and μ_w, the surface tension σ, and the gravity acceleration g, (b) the channel properties including the width W, and, (c) the inflow properties such as the inflow depth d_1, the inflow velocity V_1, a characteristic turbulent velocity u'_1, and the boundary layer thickness δ. The air-water flow properties may be expressed as :

$$C, F, V, u', d_{ab} \ldots = F_1(x, y, z, d_1, V_1, u_1', x_1, \delta, W, g, \rho_{air}, \rho_w, \mu_{air}, \mu_w, \sigma, \ldots) \quad (1)$$

where C is the void fraction, F is the bubble count rate, V is the velocity, u' is a characteristic turbulent velocity, d_{ab} is a bubble size, x is the coordinate in the flow direction measured from the nozzle, y is the vertical coordinate, z is the transverse coordinate measured from the channel centreline, and x_1 is the distance from the upstream gate (Fig. 1). In addition, biochemical properties of the water solution may be considered. If the local void fraction C is known, the density and viscosity of the air-water mixture may be expressed in terms of the water properties and void fraction only; hence the parameters ρ_{air} and μ_{air} may be ignored.

Since the relevant length scale is the upstream flow depth d_1, Equation (1) may be transformed in dimensionless terms :

$$C, \frac{F \times d_1}{V_1}, \frac{V}{\sqrt{g \times d_1}}, \frac{u'}{V_1}, \frac{d_{ab}}{d_1} \ldots = F_2\left(\frac{x}{d_1}, \frac{y}{d_1}, \frac{z}{d_1}, \frac{V_1}{\sqrt{g \times d_1}}, \frac{u_1'}{V_1}, \rho_w \times \frac{V_1 \times d_1}{\mu_w}, \rho_w \times \frac{V_1^2 \times d_1}{\sigma}, \frac{x_1}{d_1}, \frac{\delta}{d_1}, \frac{W}{d_1}\right) \quad (2)$$

In Equation (2), the dimensionless air-water flow properties (left handside terms) at a dimensionless position (x/d_1, y/d_1, z/d_1) are expressed as functions of the dimensionless inflow properties and channel geometry. In the right handside of Equation (2), the fourth, sixth and seventh terms are the inflow Froude, Reynolds and Weber numbers respectively. Any combination of these numbers is also dimensionless and may be used to replace one of the combinations. In particular one parameter can be replaced by the Morton number $Mo = g \times \mu_w^4/(\rho_w \times \sigma^3)$ and it yields:

$$C, \frac{F \times d_1}{V_1}, \frac{V}{\sqrt{g \times d_1}}, \frac{u'}{V_1}, \frac{d_{ab}}{d_1} \ldots = F_3\left(\frac{x}{d_1}, \frac{y}{d_1}, \frac{z}{d_1}, Fr_1, \frac{u_1'}{V_1}, Re_1, Mo, \frac{x_1}{d_1}, \frac{\delta}{d_1}, \frac{W}{d_1}\right) \quad (3)$$

where Fr_1 and Re_1 are respectively the inflow Froude and Reynolds numbers. The Morton number is a function only of fluid properties and gravity constant, and it becomes an invariant if the same fluids (air and water) are used in both model and prototype, as in the present study.

In a geometrically similar model, a true dynamic similarity is achieved if and only if each dimensionless parameter has the same value in both model and prototype. Scale effects may exist when one or more dimensionless terms have different values between model and prototype.

In the study of open channel flows including the hydraulic jump, a Froude similitude is commonly used because the gravity effects are dominant (e.g. Henderson 1966, Chanson 1999,2004). That is, the model and prototype Froude numbers must be equal. However the entrapment of air bubbles and the mechanisms of air bubble breakup and coalescence are dominated by surface tension effects, while turbulent processes in the shear region are dominated by viscous forces (Wood 1991, Chanson 1997). Dynamic similarity of air bubble entrainment in hydraulic jumps becomes impossible because of too many relevant

parameters (Froude, Reynolds and Morton number) in Equation (3). For example, with the same fluids (air and water) in model and prototype, the air entrainment process is adversely affected by significant scale effects in small size models (Kobus 1984). Figure 2 illustrates two hydraulic jumps with identical inflow Froude numbers but different inflow Reynolds numbers. In the smaller channel (Fig. 2A), drastically lesser bubble entrainment was observed.

It is worth noting that the above analysis does not account for the characteristics of the instrumentation. The type of instrumentation, the size of the probe sensor, the sampling rate and possibly other probe characteristics do affect the minimum bubble size detectable by the instrumentation. In the particular case of phase-detection intrusive probes, bubble chords smaller than the probe sensor cannot be detected while bubble chord times smaller than the scan period (i.e. inverse of sampling rate) are not recorded. To date most systematic studies of scale effects affecting air entrainment processes were conducted with the same instrumentation and sensor size in all experiments. That is, the probe sensor size was not scaled down in the small size models. The present study is no exception but it is acknowledged that this aspect might become a constraint and limitation.

(A) Fr_1 = 5.1, Re_1 = 2.4 E+4, x_1 = 0.5 m, W = 0.25 m (shutter speed: 1/60 s)

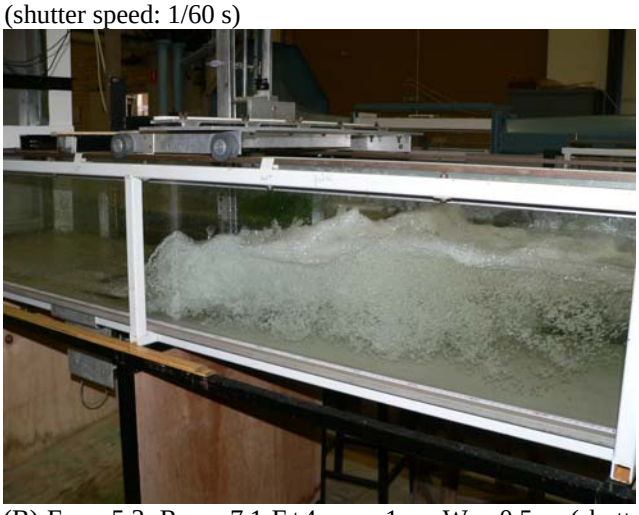

(B) Fr_1 = 5.3, Re_1 = 7.1 E+4, x_1 = 1 m, W = 0.5 m (shutter speed: 1/80 s)

Figure 2: Photographs of air bubble entrainment in hydraulic jumps for Fr_1 = 5.

Experimental Facilities

New experiments were performed in the Gordon McKay Hydraulics Laboratory at the University of Queensland (Table 1, Fig. 2 & 3). The first channel was horizontal, 3.2 m long and 0.25 m wide. Both bottom and sidewalls were made of 3.2 m long glass panels. This channel was previously used by Chanson (1995) and Chanson and Brattberg (2000). The second channel was horizontal, 3.2 long and 0.5 m wide. The sidewalls were made of 3.2 m long glass panels and the bed was made of 12 mm thick PVC sheet. This flume was previously used by Chanson (2005). Both channels were fed by a constant head tank. Further details on the experiments were reported in Chanson (2006).

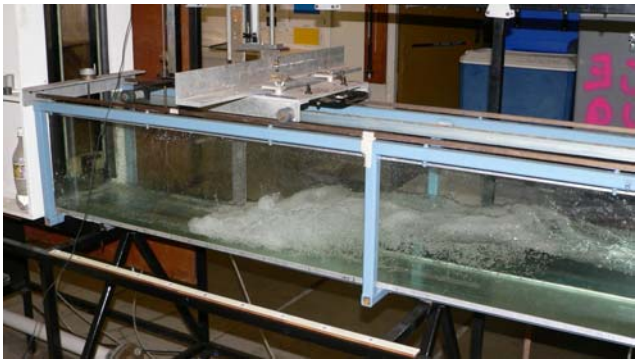

(A) Fr_1 = 8.4, Re_1 = 3.85 E+4 E+4, x_1 = 0.5 m, W = 0.25 m

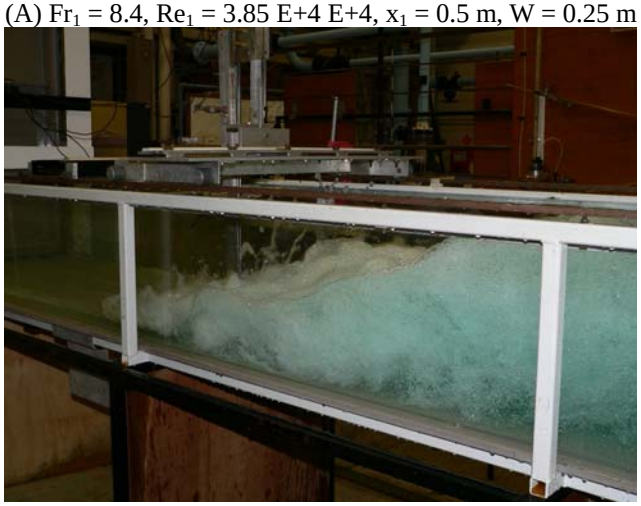

(B) Fr_1 = 8.6, Re_1 = 9.8 E+4, x_1 = 1 m, W = 0.5 m

Figure 3: Photographs of air bubble entrainment in hydraulic jumps for Fr_1 = 8.5 (shutter speed: 1/80 s).

Instrumentation

The flow rate was measured with a 90º V-notch weir calibrated on-site with a volume-per-time technique in the small flume. In the 0.5 m wide channel, the water discharge was measured with a Venturi meter calibrated in-situ with a large V-notch weir. The percentage of error was expected to be less than 2%. The water depths were measured using rail mounted pointer gauges with an accuracy of 0.2 mm.

The air-water flow properties were measured with a single-tip conductivity probe (needle probe design). The probe consisted of a sharpened rod (platinum wire ∅ = 0.35 mm) which was insulated except for its tip and set into a metal supporting tube. It was excited by an electronic system (Ref. AS25240) designed with a response time less

than 10 μs and calibrated with a square wave generator. The probe vertical position was controlled by a fine adjustment system with an accuracy of 0.1 mm.
Additional informations were obtained with some digital cameras Panasonic™ Lumix DMC-FZ20GN (shutter: 8 s to 1/2,000 s) and Olympus™ Camedia C700 (shutter: 4 s to 1/1,000 s).

Quality control, sampling rate and duration

Phase-detection probes are very sensitive devices and they are susceptible to a number of problems. In the present study, the quality control procedure developed by Toombes (2002, pp. 70-72) was applied thoroughly. Specifically, the probe signals were checked systematically for (a) long-term signal decays often induced by probe tip contamination, (b) short-term signal fluctuations caused by debris and water impurities, (c) electrical noise and (d) non-representative samples. While most quality control procedure can be automatised, it must be stressed that human supervision and intervention are essential to validate each quality control step.
The sampling rate and probe sensor size determines the resolution of the intrusive phase-detection probe, in particular in terms of bubble count rate and chord sizes. A sensitivity analysis was performed systematically on the effects of sampling duration T_{scan} and sampling rate F_{scan} on some hydraulic jump air-water properties, namely the void fraction and bubble count rate. The sampling time was selected within the range 0.7 s ≤ T_{scan} ≤ 300 s and the sampling frequency was between 600 Hz ≤ F_{scan} ≤ 80 kHz. Typical results are shown in Figure 4. First the data showed that the sampling rate had almost no effect on the void fraction for a given sampling duration. However the bubble count rate was underestimated for sampling rates below 5 to 8 kHz (Fig. 4A). Herein a sampling rate of 20 kHz was used for all the study. Second, the sampling duration had little effect on both void fraction and bubble count rate for scan periods longer than 30 to 40 s (Fig. 4B). In the present study, the typical scan duration was 45 s.
In the recirculation region, some scatter in terms of void fraction and bubble count rate was observed for sampling periods below 70 to 100 seconds. These were believed to be caused by the fluctuations in jump toe position, with typical observed frequencies of 0.5 to 2 Hz. Lastly it must be stressed that the present findings were specific to the hydraulic jump measurements with the single-tip conductivity probe.

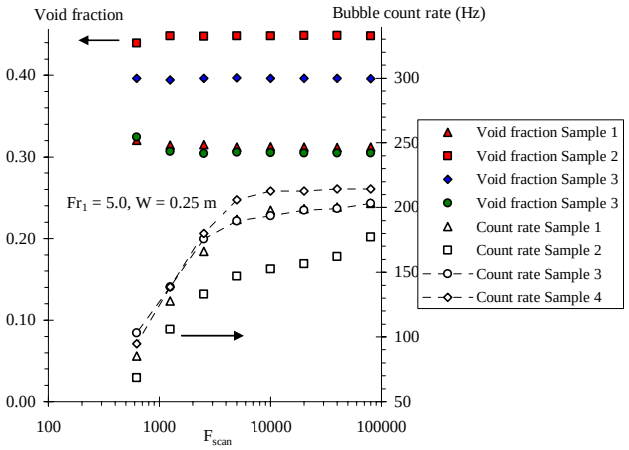

(A) Effects of sampling rate on void fraction and bubble count rate for T_{scan} = 45 s

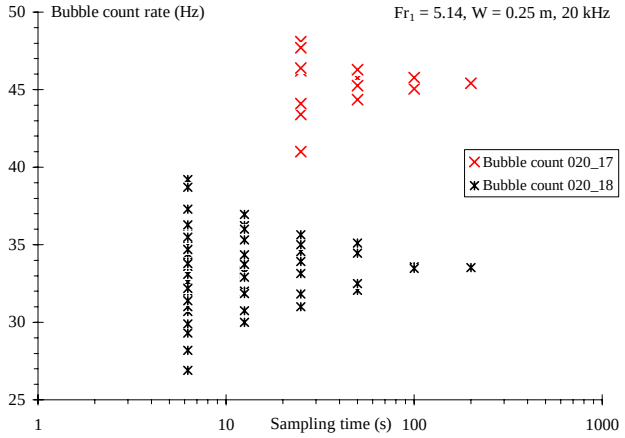

(B) Effects of sampling duration on bubble count rate for a scan rate of F_{scan} = 20 kHz

Figure 4: Effects of sampling rate and duration on the air-water flow measurements in hydraulic jump.

Inflow conditions and experimental flow conditions

Clear-water velocity measurements were performed in both flumes using a Prandtl-Pitot tube (∅= 3.3 mm). The results showed that the supercritical inflow was partially-developed for all investigated flow conditions (Table 1). The relative boundary layer thickness δ/d_1 was about 0.5 to 0.6 depending upon the inflow conditions.
The two channels were designed to be geometrically similar based upon a Froude similitude with undistorted scale. The geometric scaling ratio was L_r = 2.0 between the narrow and wide channels, where L_r is the ratio of prototype to model dimensions. Similar experiments were conducted for identical Froude numbers Fr_1, relative channel width W/d_1 and relative gate-to-jump toe distance x_1/d_1 (Fig. 2 & 3). Measurements were performed at identical cross-sections $(x-x_1)/d_1$ in both channels with two inflow Froude numbers (Table 1). All measurements were conducted on the channel centreline. Hence Equation (3) was studied with only one dependant variable, namely the inflow Reynolds number Re_1. The present study was focused in the developing air-water flow region: i.e., $(x-x_1)/d_1 \leq 25$.
In addition, the effect of the relative width W/d_1 was tested for two Froude numbers at large inflow Reynolds numbers (Table 1).

Table 1: Experimental flow conditions.

	Fr_1 $V_1/\sqrt{g\times d_1}$	Re_1 $\rho\times V_1\times d_1/\mu$	W/d_1	Remarks
Small channel	5.1	2.5 E+4	19	W = 0.25 m
	8.4	3.85 E+4	19	
	5.0	7.7 E+4	9	
	8.0	9.5 E+4	10	
Large channel	5.1	6.8 E+4	19	W = 0.5 m.
	8.6	9.8 E+4	21	

Basic Air-Water Flow Patterns

A hydraulic jump is the rapid transformation from rapid to fluvial flow motion. The sudden transition is characterised by the development of large-scale turbulence, surface waves and spray, energy dissipation and air entrainment. Air bubbles and air packets are entrained at the jump toe into a free shear layer characterised by intensive turbulence production, predominantly in vortices with horizontal axes perpendicular to the flow direction (Fig. 2 & 3). Air entrainment occurs in the form of air bubbles and air pockets entrapped at the impingement of the upstream jet flow with the roller. The air packets are broken up in very small air bubbles as they are entrained in the shear region which is characterised by large air content and maximum bubble count rates. Once the entrained bubbles are advected into regions of lesser shear, bubble collisions and coalescence lead to larger air entities (bubbles, pockets) that are driven by buoyancy towards the free-surface.

Air can be entrained by a combination of different mechanisms. If the inflow is aerated upstream of the intersection with the pool of water, the aerated layer at the jet free-surface is entrained past the impingement point. This process is also called pre-entrainment or two-phase flow air flux. Further an air layer is set into motion by shear friction next to the free-surface of the impinging flow and some air is trapped at the entrainment point. Another mechanism is the aspiration of the induction trumpet formed at the intersection of the water jet with the roller (i.e. jump toe). At the closure of the trumpet, air packets are entrapped and entrained within the shear flow (e.g. Chanson and Brattberg 1998).

In the recirculation region above the mixing layer, strong unsteady flow reversals occur. During the present study, the location of the jump toe was consistently fluctuating around its mean position and some "vortex shedding" developed in the mixing layer. High-speed photographs showed a significant number of air-water ejections above the mean "free-surface" of the roller (Fig. 5). The ejected packets re-attached rapidly to the jump roller and they were not always observed by eye. The bulk of the roller was further enhanced by the volume of entrained air. Visual observations suggested that the maximum roller height was about 10 to 20% larger than the downstream flow depth (i.e. conjugate depth) depending upon the inflow Froude numbers and experimental conditions. Further photographic evidences were presented in Chanson (2006).

The position of the hydraulic jump toe fluctuated with time within a 0.2 m to 0.4 m range depending upon the flow conditions. Pulsation frequencies F_{toe} of the jump toe were typically about 0.5 Hz to 2 Hz for the present study. In terms of the Strouhal number $F_{toe}\times d_1/V_1$, the present data were close to the observations of Long et al. (1991) and Mossa and Tolve (1998). These jump toe pulsations were believed to be caused by the growth, advection and pairing of large scale vortices in the developing shear layer of the jump (Habib et al. 1994).

(A) Fr_1 = 6.7, Re_1 = 9.4 E+4, x_1 = 1 m, W = 0.25 m

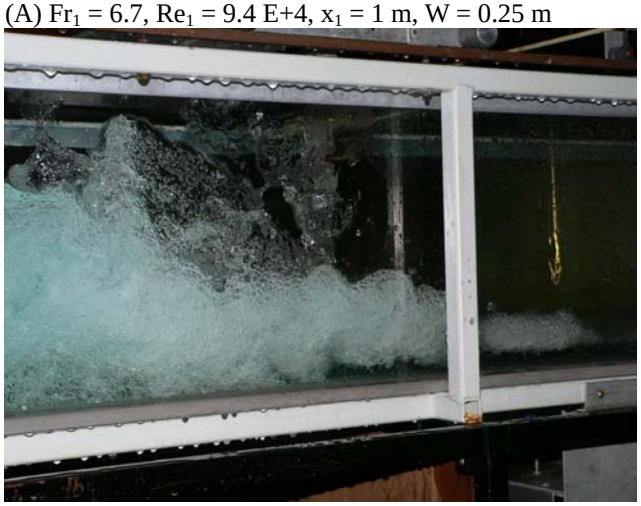

(B) Fr_1 = 8.6, Re_1 = 9.8 E+4, x_1 = 1 m, W = 0.5 m

Figure 5: High-shutter speed of air-water structures in hydraulic jumps with partially-developed inflow conditions (shutter speed: 1/1,000 s).

Effects of the inflow Reynolds number and relative width

When experiments with identical inflow Froude numbers were repeated in both channels, the hydraulic jump flows appeared visually more energetic in the large flume at the larger Reynolds number. This was seen using high-shutter speed photographs (Fig. 2 & 3). Figures 2A and 3A show the photograph in the small flume. Little air-water projections and comparatively larger entrained air bubbles were observed. Figures 2B and 3B illustrate the same jumps in the large channel with identical inflow Froude numbers but larger Reynolds numbers. The amount of air-water projections above the jump roller was larger at the highest Reynolds number (Fig. 5). This was associated with significant spray, splashing and waves that sometimes overtopped the channel walls. During these experiments, some spray droplets were seen at heights of more than 0.5 to 1 m above the channel bed in the large flume. In contrast, little spray was observed in the small channel.

Air-Water Flow Properties

A hydraulic jump with partially-developed inflow is characterised by a turbulent shear layer with an advective diffusion region in which the air concentration distributions exhibit a peak in the turbulent shear region (Resch and Leutheusser 1972, Chanson 1995, Chanson and Brattberg 2000, Murzyn et al. 2005). This feature is sketched in Figure 1. The bubble diffusion region is very similar to that observed in two-dimensional plunging jet flows (Cummings and Chanson 1997a,b, Brattberg and Chanson 1998).

A similar advective diffusion layer was observed in the present study and it is documented experimentally in Figure 6. The void fraction distributions exhibited typically a characteristic peak C_{max} in void fraction which decreased with increasing distance ($x-x_1$) from jump toe, while the diffusion layer broadened. The interactions between developing shear layer and air diffusion layer are complicated, and they are believed to be responsible for the existence of a peak F_{max} in bubble count rate seen in Figure 6 and 7. Experimental observations showed that the location where $F = F_{max}$ did not coincide with the locus of maximum void fraction (Fig. 6).

In the air diffusion layer, the analytical solution of the advective diffusion equation for air bubbles yields the void fraction profile (Chanson 1997, Cummings and Chanson 1997a):

$$C = \frac{\frac{Q_{air}}{Q_w}}{\sqrt{4 \times \pi \times D^{\#} \times \frac{x - x_1}{d_1}}} \times \left(\exp\left(- \frac{\left(\frac{y}{d_1} - 1\right)^2}{4 \times D^{\#} \times \frac{x - x_1}{d_1}} \right) + \exp\left(- \frac{\left(\frac{y}{d_1} + 1\right)^2}{4 \times D^{\#} \times \frac{x - x_1}{d_1}} \right) \right) \quad (4)$$

where Q_{air} is the volume flow rate of entrained air, Q_w is the water discharge, $D^{\#}$ is a dimensionless diffusivity: $D^{\#} = D_t/(V_1 \times d_1)$, D_t is the turbulent diffusivity which averages the effects of turbulent diffusion and of longitudinal velocity gradient. Equation (4) is valid for both two-dimensional supported plunging jet and hydraulic jump flows. In practice, experimental data showed that the void fraction profiles were best predicted by an approximate expression :

$$C = C_{max} \times \exp\left(- \frac{\left(\frac{y}{d_1} - \frac{Y_{C\,max}}{d_1}\right)^2}{4 \times D^{\#} \times \frac{x - x_1}{d_1}} \right) \quad (5)$$

where C_{max} is the maximum air content in the turbulent shear layer region measured at $y = Y_{Cmax}$ above the bottom (Fig. 1). Equation (5) is compared with experimental data in Figure 6. The values of C_{max} and $D^{\#}$ were deduced from the best data fit. Overall, the order of magnitude was consistent with the earlier studies of Chanson (1995) and Chanson and Brattberg (2000).

In the present study, Equation (5) was observed only for inflow Reynolds numbers $Re_1 > 2.5$ E+4. For lower inflow Reynolds numbers, the rate of air entrainment was weak and rapid air detrainment destroyed any organised advective diffusion layer (Fig. 7).

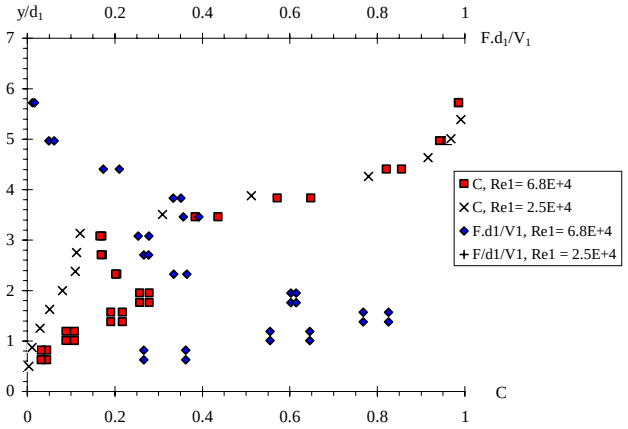

(A) $Fr_1 = 5$, $W/d_1 = 19$, $(x-x_1)/d_1 = 7.5$

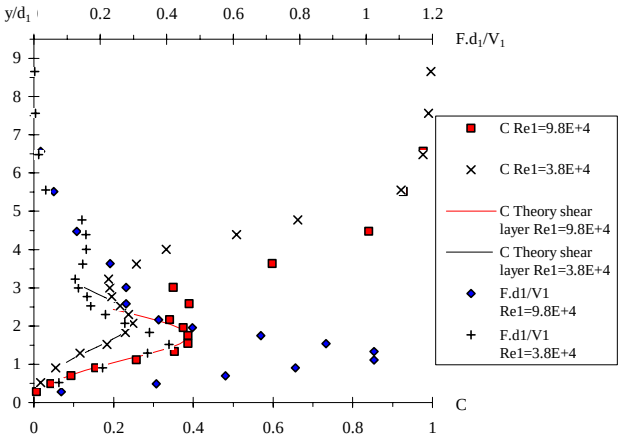

(B) $Fr_1 = 8.5$, $W/d_1 = 19$, $(x-x_1)/d_1 = 4$

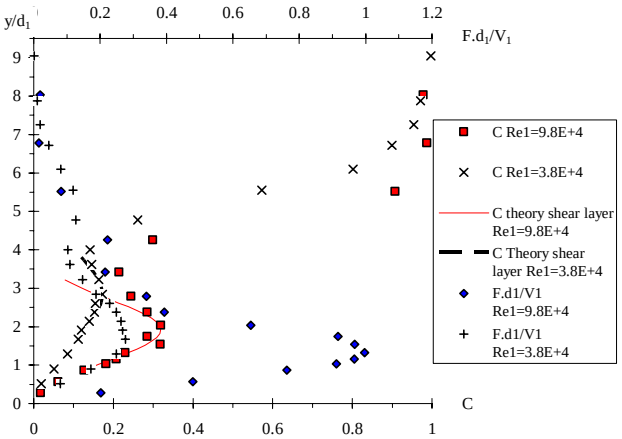

(C) $Fr_1 = 8.5$, $W/d_1 = 19$, $(x-x_1)/d_1 = 12$

Figure 6: Dimensionless distributions of void fraction and bubble count rate in hydraulic jumps with partially-developed inflow conditions. Comparison between small and large channel data, and Equation (5).

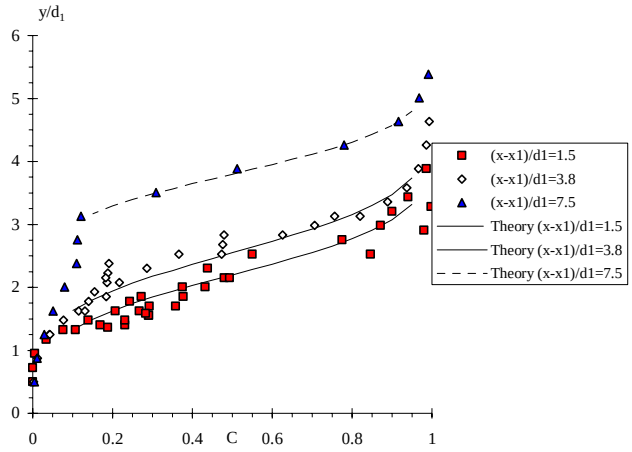

Figure 7: Dimensionless distributions of void fraction in the small channel Fr_1 = 5. Fr_1 = 5.1, Re_1 = 2.5 E+4, x_1 = 0.5 m, W = 0.25 m. Comparison with Equation (6).

Upper free-surface region

In the upper region of the roller, the void fraction distributions tended to follow a solution of the bubble advection equation for a free-jet :

$$C = \frac{1}{2} \times \left(1 + \text{erf}\left(\frac{1}{2} \times \sqrt{\frac{V_1}{D_t'}} \times \frac{y - Y_{50}}{\sqrt{x - x_1}}\right)\right) \quad (6)$$

where Y_{50} is the characteristic depth where the void fraction is 50%, D_t' is the turbulent diffusivity of the upper interface and erf is the Gaussian error function. Equation (6) was first derived by Chanson (1989) for water jets discharging into air (Chanson 1997, Brattberg et al. 1998). Note that D_t' characterises the air bubble diffusion process at the upper free-surface while, in Equations (4) and (5), the diffusivity D_t describes the advective diffusion process in the air-water shear layer downstream of a point source at $x = x_1$ and $y = d_1$ (i.e. jump toe).
Strictly speaking, Equation (6) is not applicable to a hydraulic jump roller "free-surface", although it does fit the data (Murzyn et al. 2005, Chanson 2006) (Fig. 7). It is shown in Figure 7 for curiosity.

Effects of Reynolds number and relative channel width

Similar experiments were repeated with identical inflow Froude numbers Fr_1 and relative channel width W/d_1, but different inflow Reynolds numbers Re_1 (Table 1). The results allowed testing the validity of Equation (3). They showed systematically that the void fraction distributions had a similar shape in the advective diffusion layer, but for $Re_1 < 2.5$ E+4. For the lowest inflow Reynolds number, the upward advection of air bubbles towards the free-surface was dominant and the advective diffusion layer was destroyed by the buoyancy effects (Figure 7). At larger Reynolds numbers, the void faction profiles showed some self-similarity, but the longitudinal variations in void fraction distributions indicated a more rapid de-aeration of the jump associated with an upward shift of the advective diffusion layer at the lower Reynolds numbers for an identical Froude number and relative channel width (Fig. 6).
Importantly, all the experiments showed some drastically smaller dimensionless bubble count rates at the lower Reynolds numbers, particularly in the air-water mixing layer. This is seen in Figure 6, where the maximum bubble count rate in the shear layer was typically 2 to 3 times smaller in the small channel for the lower Reynolds number. For example, for Fr_1 = 5 and Re_1 = 2.5 E+4, the dimensionless bubble count rate $F_{max} \times d_1/V_1$ was nearly 1/3rd of that measured in the larger flume with Fr_1 = 5 and Re_1 = 9.4 E+4 (Fig. 6A). For Fr_1 = 8.5, the dimensionless bubble count rates in the smaller experiment were about half of those recorded at larger Reynolds number in the large flume (Fig. 6B & 6C).
Basically, present experiments demonstrated consistently some scale effects in terms of void fraction and bubble count rate distributions in the smaller experiments with $Re_1 < 4$ E+4 for identical Froude numbers Fr_1 and relative channel width W/d_1.
In addition, some experiments were performed with identical inflow Froude and Reynolds numbers but with a different relative channel width W/d_1 (Table 1). A comparison showed no effect of the channel width on the distributions of void fraction and bubble count rate, as well as in terms of bubble chord time distributions within $8 \leq W/d_1 \leq 22$ and for 0.25 m ≤ W ≤ 0.50 m.

Bubble/Drop Chord Time Distributions

Bubble chord times were recorded for a range of flow conditions. The bubble chord time is proportional to the bubble chord length and inversely proportional to the velocity. In a complicated flow such as a hydraulic jump where flow reversal and recirculation exist, the phase-detection intrusive probe cannot discriminate accurately the direction or magnitude of the velocity. Hence only air/water chord time data are presented. Further the air/water chord times are shown in milliseconds. For a 1 m/s particle velocity, a 1 ms chord time would correspond to a 1 mm particle chord length.
Figures 8 and 9 show typical normalised bubble chord time distributions for two inflow Froude numbers. In each figure, the legend provides the location (x-x_1, y/d_1), local air-water flow properties (C, F), and number of recorded bubbles N_{ab}. The histogram columns represent each the probability of droplet chord time in a 0.5 ms chord time interval. For example, the probability of bubble chord time from 1 to 1.5 ms is represented by the column labelled 1 ms. Bubble chord times larger than 15 ms are regrouped in the last column (> 15).
First, the results highlighted the broad spectrum of bubble chord time at each location. The range of bubble chord time extended over several orders of magnitude, including at low void fractions, from less than 0.1 ms to more than 30 ms (Fig. 8).
Second the distributions were skewed with a preponderance of small bubble chord time relative to the mean. For example, in Figure 8, the mode was about 0.5 to 1.5 ms. The probability distribution functions of bubble chord time tended to follow in average a log–normal distribution. Note that a similar finding was observed in plunging jet flows with freshwater and seawater (e.g. Cummings and Chanson 1997b, Chanson et al. 2004,2006).
Third, let us observe that the bubble chord time distributions had a similar shape at most locations y/d_1 although the air-water structures may differ substantially between the air-water shear layer and the recirculation region above.

The shape of vertical distributions of median chord times was close to some vertical distribution of mean Sauter diameter presented by Murzyn et al. (2005). In that study, bubble chord times were transformed into bubble diameter using the time-average velocity measured with a dual-tip optical fibre probe.

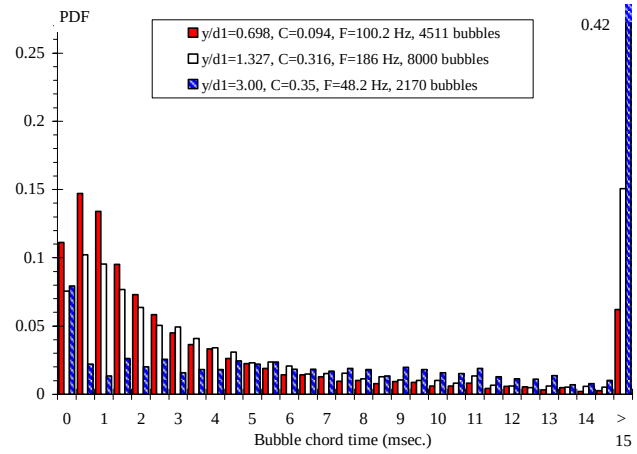

(A) $x\text{-}x_1$ = 0.20 m

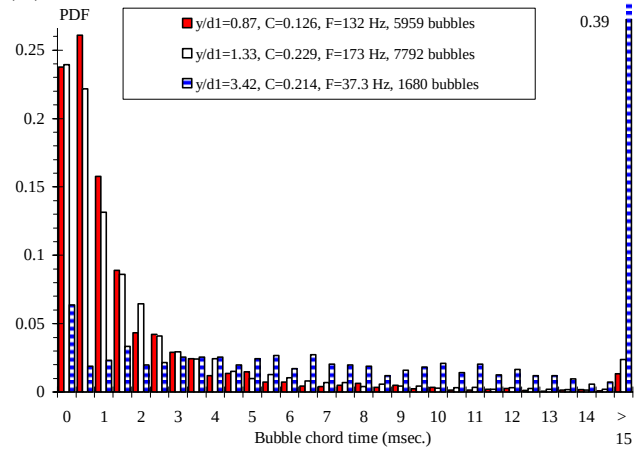

(B) $x\text{-}x_1$ = 0.30 m

Figure 8: Bubble chord time distributions in the bubbly flow region: Fr_1 = 8.5, Re_1 = 9.8 E+4, d_1 = 0.024 m, x_1 = 1.0 m, W = 0.50 m, 0.5 ms chord time intervals.

Effects of inflow Reynolds numbers and channel width

Similar experiments were repeated with identical inflow Froude numbers Fr_1 and relative channel width W/d_1, but different inflow Reynolds numbers Re_1. The results showed systematically that the bubble chord time distributions had a similar shape for all Reynolds numbers. Quantitatively, the bubble chord times were similar (Fig. 9). That is, the chord times were not scaled by the geometric scaling ratio L_r = 2, as they should for a true dynamic similarity based upon a Froude similitude. In the small channel, a Froude similitude would imply that the bubble chord times be 1/2 smaller than in the large model for L_r = 2. Further, the bubble chord time distributions at the larger Reynolds numbers were comparatively broader than those at low Reynolds numbers for an identical inflow Froude number and identical locations (i.e. $(x\text{-}x_1)/d_1$, y/d_1).
Figure 9 shows a comparison of bubble chord time distributions for identical inflow Froude number and relative channel width at two characteristic locations : i.e., $y = Y_{Fmax}$ and $y = Y_{Cmax}$ corresponding respectively to the elevations where the bubble count rate was maximum and the void fraction was maximum in the advective diffusion layer.
In the present study, some experiments were performed also with identical inflow Froude and Reynolds numbers but with a different relative channel width W/d_1. A comparison of bubble chord time distributions showed basically no effect of the channel width on the chord time distributions.

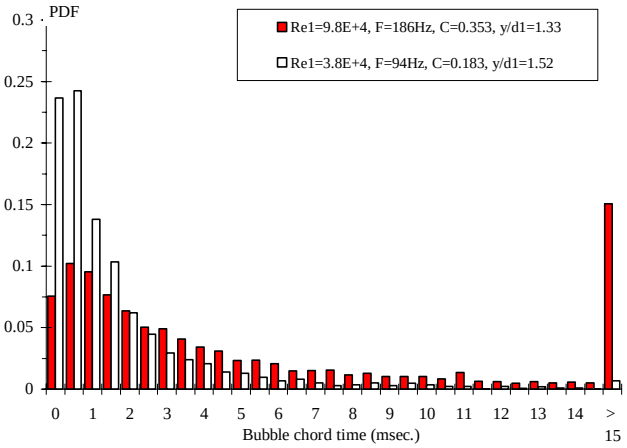

(A) Comparison at location where the bubble count rate is maximum $F = F_{max}$

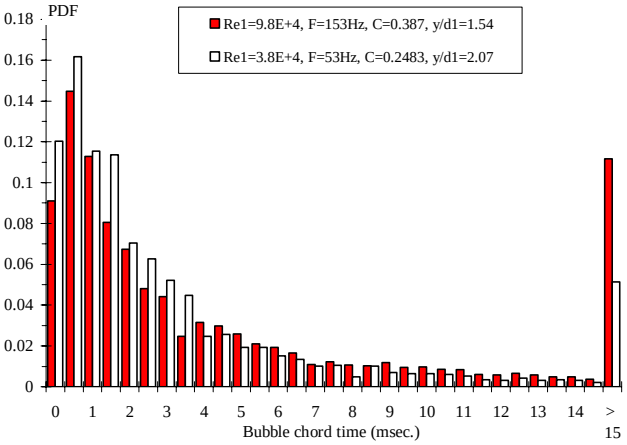

(B) Comparison at location where the void fraction is maximum $C = C_{max}$ in the advective diffusion layer

Figure 9: Bubble chord time distributions in the bubbly flow region: Fr_1 = 8.5, d_1 = 0.024 m, x_1/d_1 = 40, $(x\text{-}x_1)/d_1$ = 12, W/d_1 = 20, 0.5 ms chord time intervals. Comparison between Re_1 = 3.8 E+4 and 9.8 E+4.

Water chord data in upper spray/mist region

Visual observations showed a substantial amount of air-water projections and splashing above the roller, particularly at large Reynolds numbers. Most splashing structures were water and water-and-air packets surrounded by air (Fig. 5). Herein the upper spray/mist region is commonly defined as the air-water region in which the liquid fraction is less than 10% (i.e. C > 0.90).
Figure 10 shows some typical droplet chord time distributions at various positions in the upper spray region above the roller. For each graph, the caption provides the local air-water flow properties (C, F) and the number of recorded droplets N_{ab} during the scan period (T_{scan} = 45 s). The histogram columns represent each the probability of

droplet chord time in a 0.5 ms interval.
First, the results highlighted a broad spectrum of droplet chord time at each location (Fig. 10). The range of drop chord times extends over several orders of magnitude from less than 0.5 ms to more than 15 ms. Such a range would correspond to tiny droplets flowing at high velocity to large water packets moving at low speed past the probe.
Second the number of droplets was small at low liquid fractions. The finding implies that longer sampling durations would be required to gain a more thorough description of the spray/mist statistical properties.
Third, the probability distribution functions of water chord times were fairly flat and quasi-uniform. They did not follow the skewed log-normal distribution shape observed for $0.7 < C < 0.9$ (Chanson 2006).
In the spray region, drop formation results from surface distortion, tip-streaming of ligaments and interactions between eddies and free-surface (e.g. Hoyt and Taylor 1977, Rein 1998). The formation and ejection of a droplet must be associated with a transfer of turbulent kinetic energy from the main flow. Once a droplet is ejected, its ejection process is the dominant effect because the droplet response time is nearly two orders of magnitude larger than the air flow response time. The energy of each droplet is a combination its potential energy and kinetic energy, although Nielsen (2004, Pers. Comm.) suggested possibly some pressure increase induced by surface tension.

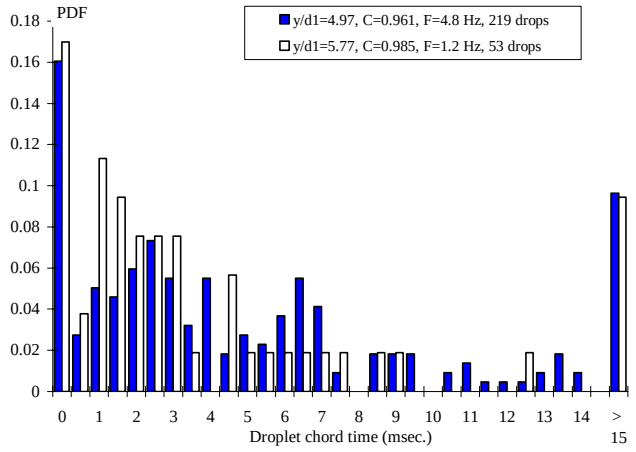

(A) $Fr_1 = 5.1$, $Re_1 = 6.8$ E+4, $d_1 = 0.0265$ m, $x_1 = 1.0$ m, W = 0.50 m, $x\text{-}x_1 = 0.2$ m

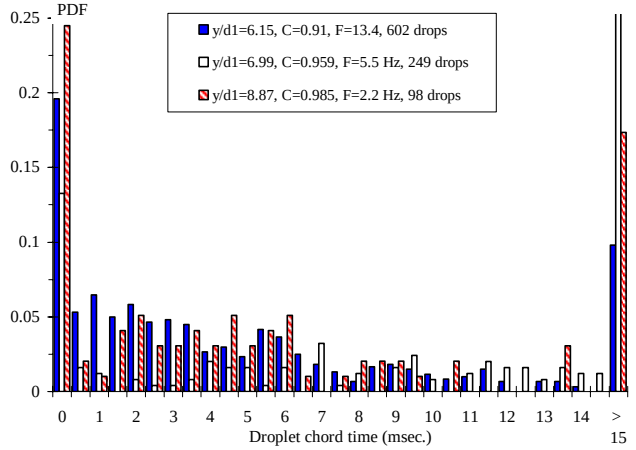

(B) $Fr_1 = 8.5$, $Re_1 = 9.8$ E+4, $d_1 = 0.025$, $x_1 = 1.0$ m, W = 0.50 m, $x\text{-}x_1 = 0.4$ m

Figure 10: Droplet chord time distributions in the upper spray/mist region.

Discussion

The present results demonstrated that the dynamic similarity of air bubble entrainment in hydraulic jump was not satisfied with a Froude similitude and a geometric scaling ratio of $L_r = 2$ (i.e. 2:1). Significantly smaller bubble count rates and comparatively larger bubble chord times were observed in the small channel operating at lower Reynolds number for an identical inflow Froude number. Are there other scaling criteria, beside the Froude similitude, in such a case?
Equation (3) showed that the present study was performed with only one dependant variable, namely the Reynolds number Re_1. All the other dependant parameters were controlled and maintained constant including the inflow Froude number Fr_1, the Morton number Mo, the relative width W/d_1, the inflow conditions x_1/d_1 and δ/x_1, and the measurement location ($(x\text{-}x_1)/d_1$, y/d_1, $z/d_1=0$).
An alternative approach could be based upon a Reynolds similitude. A relevant hydraulic jump study is the work of Rouse et al. (1959) in a wind tunnel. In this study, the air flow was selected to conduct turbulence measurements with a hot-wire probe in the shear flow. While the findings of Rouse et al. (1959) were important, it was argued that their air model did not reproduce all the main features of the hydraulic jump (Rajaratnam 1965). For example, a comparison between the air flow results of Rouse et al. (1959) and the water flow data of Resch and Leutheusser (1972b) highlights some differences in terms of distributions of normal and tangential Reynolds stresses in the jump flow.
In summary, the dynamic similarity of air entrainment in hydraulic jumps is characterised by a large number of relevant parameters. Neither the Froude similitude nor Reynolds similitude are free of scale effects, unless the physical modelling is conducted at full-scale.

Conclusions

In the present study, similar experiments were conducted in hydraulic jumps with identical inflow Froude numbers Fr_1 and relative channel width W/d_1 using a geometric scaling ratio of 2:1 (Table 1). The study was further conducted with two relative channel widths W/d_1. Detailed air-water flow measurements were performed with a phase-detection intrusive probe in two channels.
The void fraction distributions showed the presence of an advective shear layer in which the air content distributions followed an analytical solution of the diffusion equation. In the mixing layer, a region of very high bubble count rate was observed for all flow conditions. Present results demonstrated that the advective diffusion layer was observed only for $Re_1 > 2.5$ E+4. For smaller inflow Reynolds numbers, the bubble entrapment rate was relatively weak and the air detrainment process dominated the air detrainment and buoyancy effects.
The distributions of bubble chord times showed a broad range of entrained bubble chord times ranging over two orders of magnitude. The probability distribution functions of bubble chord times were skewed with a preponderance of chord times smaller than the mean. They followed closely a

log-law distribution at all sampling locations for C < 0.30. In the upper spray and mist region, the probability distribution functions of water droplets exhibited a relatively flat distribution over a wide range of ejected drop chord times.

The results of Froude-similar experiments showed some drastic scale effects in the smaller hydraulic jumps in terms of void fraction, bubble count rate and bubble chord time distributions. Void fraction distributions implied comparatively greater detrainment at low Reynolds numbers yielding to lesser overall aeration of the jump roller. The dimensionless bubble count rates were significantly lower in the smaller channel, especially in the mixing layer. The bubble chord times were quantitatively close in both channels, and they were not scaled according to a Froude similitude.

The present study complemented earlier studies: e.g., Mossa and Tolve (1998), Chanson and Brattberg (2000), Murzyn et al. (2005). It demonstrated that the hydraulic jump remains a fascinating two-phase flow that is still poorly understood. The air-water flow motion is characterised by complicated gas-liquid flow structures and strong interactions between entrained bubbles and vortical structures.

Acknowledgements

The writer thanks Graham Illidge (The University of Queensland) for his technical assistance. He acknowledges helpful discussions with Dr F. Murzyn (ESTACA Laval), Dr C. Gualtieri (University of Napoli "Federico II") and Prof. M. Mossa (Politecnico di Bari).

References

Bélanger, J.B. (1828). "Essai sur la Solution Numérique de quelques Problèmes Relatifs au Mouvement Permanent des Eaux Courantes." ('Essay on the Numerical Solution of Some Problems relative to Steady Flow of Water.') Carilian-Goeury, Paris, France (in French).

Brattberg, T., and Chanson, H. (1998). "Air Entrapment and Air Bubble Dispersion at Two-Dimensional Plunging Water Jets." Chemical Engineering Science, Vol. 53, No. 24, Dec., pp. 4113-4127. Errata : 1999, Vol. 54, No. 12, p. 1925.

Brattberg, T., Chanson, H., and Toombes, L. (1998). "Experimental Investigations of Free-Surface Aeration in the Developing Flow of Two-Dimensional Water Jets." Jl of Fluids Eng., Trans. ASME, Vol. 120, No. 4, pp. 738-744.

Chanson, H. (1989). "Study of Air Entrainment and Aeration Devices." Jl of Hyd. Res., IAHR, Vol. 27, No. 3, pp. 301-319.

Chanson, H. (1995). "Air Entrainment in Two-dimensional Turbulent Shear Flows with Partially Developed Inflow Conditions." Intl Jl of Multiphase Flow, Vol. 21, No. 6, pp. 1107-1121.

Chanson, H. (1997). "Air Bubble Entrainment in Free-Surface Turbulent Shear Flows." Academic Press, London, UK, 401 pages.

Chanson, H. (1999). "The Hydraulics of Open Channel Flow : An Introduction." Edward Arnold, London, UK, 512 pages.

Chanson, H. (2004). "Environmental Hydraulics of Open Channel Flows." Elsevier Butterworth-Heinemann, Oxford, UK, 483 pages.

Chanson, H. (2005). "Physical Modelling of the Flow Field in an Undular Tidal Bore." Jl of Hyd. Res., IAHR, Vol. 43, No. 3, pp. 234-244.

Chanson, H. (2006). "Air Bubble Entrainment in Hydraulic Jumps. Similitude and Scale Effects." Report No. CH57/05, Dept. of Civil Engineering, The University of Queensland, Brisbane, Australia, Jan., 119 pages.

Chanson, H., Aoki, S., and Hoque, A. (2004). "Physical Modelling and Similitude of Air Bubble Entrainment at Vertical Circular Plunging Jets." Chemical Engineering Science, Vol. 59, No. 4, pp. 747-754.

Chanson, H., Aoki, S., and Hoque, A. (2006). "Bubble Entrainment and Dispersion in Plunging Jet Flows: Freshwater versus Seawater." Jl of Coastal Research, Vol. 22, No. 3, May, pp. 664-677.

Chanson, H., and Brattberg, T. (1998). "Air Entrainment by Two-Dimensional Plunging Jets : the Impingement Region and the Very-Near Flow Field." Proc. 1998 ASME Fluids Eng. Conf., FEDSM'98, Washington DC, USA, June 21-25, Paper FEDSM98-4806, 8 pages (CD-ROM).

Chanson, H., and Brattberg, T. (2000). "Experimental Study of the Air-Water Shear Flow in a Hydraulic Jump." Intl Jl of Multiphase Flow, Vol. 26, No. 4, pp. 583-607.

Cummings, P.D., and Chanson, H. (1997a). "Air Entrainment in the Developing Flow Region of Plunging Jets. Part 1 Theoretical Development." Jl of Fluids Eng., Trans. ASME, Vol. 119, No. 3, pp. 597-602.

Cummings, P.D., and Chanson, H. (1997b). "Air Entrainment in the Developing Flow Region of Plunging Jets. Part 2 : Experimental." Jl of Fluids Eng., Trans. ASME, Vol. 119, No. 3, pp. 603-608.

Habib, E., Mossa, M., and Petrillo, A. (1994). "Scour Downstream of Hydraulic Jump." Proc. Conf. Modelling, Testing & Monitoring for Hydro Powerplants, Intl Jl Hydropower & Dams, Budapest, Hungary, pp, 591-602.

Henderson, F.M. (1966). "Open Channel Flow." MacMillan Company, New York, USA.

Hoyt, J.W., and Taylor, J.J. (1977). "Turbulence Structure in a Water Jet Discharging in Air." Physics of Fluids, Vol. 20, No. 10, Pt. II, Oct., pp. S253-S257.

Kalinske, A.A., and Robertson, J.M. (1943). "Closed Conduit Flow." Transactions, ASCE, Vol. 108, pp. 1435-1447.

Kobus, H. (1984). "Local Air Entrainment and Detrainment." Proceedings of the International Symposium on Scale Effects in Modelling Hydraulic Structures, IAHR, Esslingen, Germany.

Long, D., Rajaratnam, N., Steffler, P.M., and Smy, P.R. (1991). "Structure of Flow in Hydraulic Jumps." Jl of Hyd. Research, IAHR, Vol. 29, No. 2, pp. 207-218.

Mossa, M., and Tolve, U. (1998). "Flow Visualization in Bubbly Two-Phase Hydraulic Jump." Jl Fluids Eng., ASME, Vol. 120, March, pp. 160-165.

Murzyn, F., Mouaze, D., and Chaplin, J.R. (2005). "Optical Fibre Probe Measurements of Bubbly Flow in Hydraulic Jumps" Intl Jl of Multiphase Flow, Vol. 31, No. 1, pp. 141-154.

Rajaratnam, N. (1962). "An Experimental Study of Air Entrainment Characteristics of the Hydraulic Jump." Jl of Instn. Eng. India, Vol. 42, No. 7, March, pp. 247-273.

Rajaratnam, N. (1965). "The Hydraulic Jump as a Wall Jet." Jl of Hyd. Div., ASCE, Vol. 91, No. HY5, pp. 107-132. Discussion : Vol. 92, No. HY3, pp. 110-123 & Vol. 93, No. HY1, pp. 74-76.

Rein, M. (1998). "Turbulent Open-Channel Flows : Drop-Generation and Self-Aeration." Jl of Hyd. Engrg., ASCE, Vol. 124, No.1, pp. 98-102. Discussion : Vol. 125, No. 6, pp. 668-670.

Resch, F.J., and Leutheusser, H.J. (1972). "Le Ressaut Hydraulique : mesure de Turbulence dans la Région Diphasique." ('The Hydraulic Jump : Turbulence Measurements in the Two-Phase Flow Region.') Jl La Houille Blanche, No. 4, pp. 279-293 (in French).

Resch, F.J., and Leutheusser, H.J. (1972b). "Reynolds Stress Measurements in Hydraulic Jumps." Jl of Hyd. Res., IAHR, Vol. 10, No. 4, pp. 409-429.

Rouse, H., Siao, T.T., and Nagaratnam, S. (1959). "Turbulence Characteristics of the Hydraulic Jump." Transactions, ASCE, Vol. 124, pp. 926-950.

Thandaveswara, B.S. (1974). "Self Aerated Flow Characteristics in Developing Zones and in Hydraulic Jumps." Ph.D. thesis, Dept. of Civil Engrg., Indian Institute of Science, Bangalore, India, 399 pages.

Toombes, L. (2002). "Experimental Study of Air-Water Flow Properties on Low-Gradient Stepped Cascades." Ph.D. thesis, Dept of Civil Engineering, The University of Queensland.

Wisner, P. (1965). "Sur le Rôle du Critère de Froude dans l'Etude de l'Entraînement de l'Air par les Courants à Grande Vitesse." ('On the Role of the Froude Criterion for the Study of Air Entrainment in High Velocity Flows.') Proc. 11th IAHR Congress, Leningrad, USSR, paper 1.15 (in French).

Wood, I.R. (1991). "Air Entrainment in Free-Surface Flows." IAHR Hydraulic Structures Design Manual No. 4, Hydraulic Design Considerations, Balkema Publ., Rotterdam, The Netherlands, 149 pages.

Internet references

Air entrainment in the developing flow region of two-dimensional plunging jets - Databank:
{http://www.uq.edu.au/~e2hchans/data/jfe97.html}

Air entrainment at a circular plunging jet: physical and acoustic characteristics - Internet Database :
{http://www.uq.edu.au/~e2hchans/bubble/}

Air entrainment on chute and stepped spillways :
{http://www.uq.edu.au/~e2hchans/self_aer.html}